Bulletin of the Seismological Society of America, 91, 6, pp. 1875–1881, December 2001

Distribution of Fine-Scale Mantle Heterogeneity from Observations of P_{diff} Coda

by Paul S. Earle and Peter M. Shearer

Abstract We present stacked record sections of Global Seismic Network data that image the average amplitude and polarization of the high-frequency P_{diff} coda and investigate their implications on the depth extent of fine-scale (~10 km) mantle heterogeneity. The extended 1-Hz coda lasts for at least 150 sec and is observed to a distance of 130°. The coda's polarization angle is about the same as the main P_{diff} arrival (4.4 sec/deg) and is nearly constant with time. Previous studies show that multiple scattering from heterogeneity restricted to the lowermost mantle generates an extended P_{diff} coda with a constant polarization. Here we present an alternative model that satisfies our P_{diff} observations. The model consists of single scattering from weak (~1%) fine-scale (~2 km) structures distributed throughout the mantle. Although this model is nonunique, it demonstrates that P_{diff} coda observations do not preclude the existence of scattering contributions from the entire mantle.

Introduction

Elucidating the distribution and magnitude of the mantle's fine-scale seismic structure could provide clues into its chemical makeup and convective patterns. Variations in density and velocity over distances near 10 km in the deep mantle are too small to be thermal in origin. Thus, they may supply a means to detect the chemical signature of subducting slabs and rising plumes. A deterministic model that shows the absolute locations of individual 10-km features is beyond the resolution of the highest-frequency teleseismic *P* waves. However, using observations of scattered waves one can characterize the statistics (e.g., correlation length, root mean square [rms] amplitude) of fine-scale heterogeneity within a larger volume. Here we investigate the average concentration of fine-scale mantle structure as a function of depth. This is the first step toward the development of a three-dimensional model.

Strong evidence exists for velocity and density variations in the lowermost mantle with scale lengths of tens to hundreds of kilometers. For example, the onset times of high-frequency PKP_{df} and *PKKP* precursors require scattering at or immediately above the core-mantle boundary (CMB), and $SP_{diff}KS$ waveform complexity supports the existence of a highly variable ultra-low velocity layer at the mantle's base (see Garnero [2000] for review and references). In addition, recent studies have identified three-dimensional variations in scattering strength near the CMB (e.g., Wen and Helmberger, 1998; Hedlin and Shearer, 2000; Vidale and Hedlin, 2000).

But is there also fine-scale heterogeneity in the mid-mantle? Hedlin *et al.* (1997) investigated three possible models for the distribution of fine-scale structure, including CMB topography, heterogeneity throughout the D″ layer, and heterogeneity throughout the entire mantle. They showed only the latter model satisfied observations of globally averaged PKP_{df} precursors.

In this article, we demonstrate that a model with uniformly distributed mantle scatterers also predicts the observed amplitude and polarization of P_{diff} coda. P_{diff} is observed at distances greater than ~98° and its raypath consists of two mantle legs connected by a diffraction along the CMB (Fig. 1). At low frequencies (~0.05 Hz), phase conversions and reflections at the upper-mantle discontinuities produce discrete coda arrivals (e.g., Shearer, 1991). Here we study the high-frequency P_{diff} coda (~1 Hz). At this frequency the coda is characterized by an incoherent slowly decaying wavetrain (e.g., Dainty, 1990) that primarily arises from volumetric scattering (Fig. 1).

The amplitude and polarization of P_{diff} coda provide important clues to its origin. Two recent studies demonstrate that the duration and polarization of the P_{diff} coda can be explained by multiple scattering in the lowermost mantle (Bataille and Lund, 1996; Tono and Yomogida, 1996). We build upon these studies by imaging the average amplitude and polarization behavior of P_{diff} and its coda using stacking techniques and show that these observations are consistent with a model containing scatterers distributed throughout the mantle.

Data Selection

We select seismograms from the broadband three-component traces stored in the IRIS FARM archive in the dis-

tance range 92.5° to 132.5° for earthquakes occurring from January 1989 through December 1999 with $M_w \geq 5.7$. To avoid contamination from depth phases, we only use data from earthquakes with hypocenters less than 50 km. Approximately 25,000 seismograms fit the above criteria. However, only the highest quality traces can be used to image the faint high-frequency P_{diff} signal at distances well into the shadow zone.

After bandpass filtering (0.5 to 2.5 Hz), we select a set of seismograms with *PP* signal-to-noise (STN) of at least 10 on the vertical component. We define the STN as the ratio of the maximum value in a 40-sec signal window starting at the theoretical *PP* arrival time to that in a 70-sec noise window beginning 120 sec before P_{diff}. Records with data spikes or other problems are removed by visual inspection. This selection procedure identifies the 924 seismograms used for stacking.

Amplitude Stack

We apply an envelope-function stacking technique to image the time–distance behavior of high-frequency P_{diff}. This method requires the use of a reference phase to normalize the amplitudes of the seismograms recorded by widely separated stations and from varying magnitude earthquakes. We use *PP* as a reference phase because, throughout the range that P_{diff} is observed, *PP* contains no triplications and its theoretical amplitude decreases monotonically. However, two complicating factors must be accounted for when using *PP* as a reference phase.

First, the amplitude ratio of P_{diff} and *PP* varies between events due to differences in the source-radiation pattern. These variations are reduced by range binning and stacking data from multiple events with different focal mechanisms. The smoothly decreasing P_{diff} to *PP* amplitude ratio imaged in the amplitude stack (Fig. 2) suggests differences in radiation pattern do not significantly affect our results.

Second, the P_{diff} pulse is broadened because of travel-time variations introduced by three-dimensional structure and a difference in moveout between P_{diff} and *PP*. The *P*-wave travel-time variations resulting from three-dimensional structure are typically between ± 3 sec (Earle and Shearer, 1994), and the different moveout between P_{diff} and *PP* can generate a 15-sec travel-time difference across a range bin. This pulse broadening is corrected for by convolving an empirical source time function with the theoretical seismogram before comparison to the data. This step is more fully explained in the modeling section.

The seismograms are stacked as follows:

1. The squared envelope function (Kanasewich, 1981) is calculated for each seismogram. By stacking envelope functions we avoid cancellation of incoherent arrivals. In the raw amplitude traces, the coda and background noise are uncorrelated and have zero mean. Therefore, their amplitudes combine in an rms sense. Thus, it is necessary

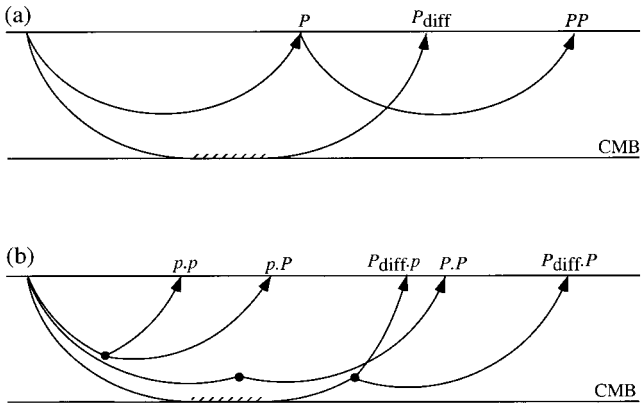

Figure 1. Cartoons illustrating the ray geometries in a flattened earth for (a) *P, PP*, and P_{diff} arrivals, and (b) scattered phases from heterogeneities in the mantle. P_{diff} is diffracted along the CMB. The scattered phases are labeled using a notation in which the source-to-scatterer and scatterer-to-receiver legs are separated by a period; *P* legs without a turning point are labeled *p*, whereas *P* legs with a turning point are labeled *P*.

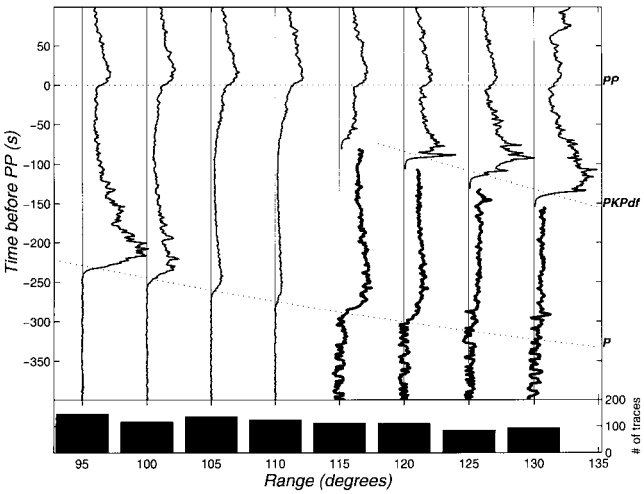

Figure 2. High-frequency P_{diff} imaged by stacking 924 vertical-component seismograms. The stacked traces are normalized to the maximum *PP* amplitude and are plotted with respect to its theoretical arrival time. To better show the small amplitude P_{diff} arrivals (heavy lines), the traces are magnified by 10 for times 20 sec before PKP_{df} at ranges greater than 112.5°. Dotted lines show the theoretical arrival time of PKP_{df}, *PP*, and P_{diff}. The number of traces in each bin is shown the histogram below the plot. The initiation of *P* before the calculated travel time primarily results from different moveout between P_{diff} that generates up to 15 sec of travel-time difference across a range bin. The increase in energy observed following *PP* in the last distance bin is *SKP*.

to square the envelope function before correcting for (subtracting) the noise level (step 2).

2. The average noise in a 70-sec time window starting 120 sec before the P_{diff} arrival is subtracted from the squared envelope function, and the trace is normalized to the maximum *PP* amplitude.
3. Weights proportional to the STN of *PP* are assigned to the traces. Traces with an amplitude *STN* greater than 20 are assigned a weight of 20.
4. The processed seismograms are aligned on the predicted *PP* onset and binned in range and time ($5^\circ \times 1$ sec). The weighted average is then calculated, converted back to amplitude, and plotted. All travel times are computed using the *iasp*91 velocity model (Kennett and Engdahl, 1991).

The resulting stack (Fig. 2) images several features of the high-frequency wave field preceding *PP*. The most relevant features to this study are the *P* and P_{diff} arrivals. The *iasp*91 model predicts *P* energy will begin diffracting around the outer core at a source–receiver distance of 98.4°. Thus, the trace plotted at 95°, which includes data from 92.5° to 97.5°, consists of direct *P* energy. The *P* arrival has significant coda, taking about 100 sec to reduce to half the maximum amplitude. Near-surface scattering produces the majority of the observed *P* coda (e.g., Dainty, 1990) and must be accounted for when modeling deeper structure. As explained in detail in the modeling section, we account for the near-surface effects by convolving our synthetics with an empirical source time function before comparing them to the data.

P_{diff} is imaged in the traces plotted at 100° and beyond. Its rise time increases, and its coda becomes more predominant at greater distances. This increase in the ratio of coda to direct arrival amplitude is the main observation indicating scattering contributions unrelated to structure near the source and receiver. If the scattering was solely due to near-surface structure then the coda decay rate would be independent of range because both the main arrival and the near-surface scattered energy would experience the same amplitude reduction from geometrical spreading, anelastic attenuation, and core diffraction. However, if the later-arriving scattered energy followed a path in which less or no amplitude reduction results from core diffraction then the relative coda amplitude would increase.

The total length of the P_{diff} coda cannot be determined because precursors to *PP* and *PKP* truncate it after about 150 sec. Precursors to *PP* are seen rising from the P_{diff} coda approximately 100 sec before *PP* between 100° and 110°. King *et al.* (1975) show these precursors likely result from scattering in the uppermost mantle. PKP_{df} and PKP_{cd} are seen at distances beyond 115°. PKP_{df} refracts through the inner core, and PKP_{cd} reflects from its surface. The traveltime curve for PKP_{cd} is not seen because it arrives no more than 2 sec after PKP_{df} in the imaged distance range.

Polarization Stack

Estimates of the ray parameter of the coda obtained from its polarization angle reduce the number of possible origins for the scattered energy. The global average polarization in the radial vertical plane of P_{diff} and the surrounding teleseismic wave field is obtained using a time-domain stacking technique. As with previous time-domain methods (e.g., Jurkevics, 1988) the polarization parameters (angle and linearity) in a given time window are determined using eigenvalue decomposition of the particle-motion covariance matrix.

The eigenvalues and eigenvectors of this matrix define an ellipse that is the least-squares best fit to the particle motion. The offset of the major axis of the ellipse from vertical is the polarization angle, and the linearity is one minus the square root of the ratio of the minor- to major-axis length. Earle (1999) gives full details of method used here. Figure 3 captures the polarization angle and linearity of the phases seen in the amplitude stack (Fig. 2).

For steeply arriving *P* energy, the polarization angle is within a few degrees of the incidence angle (Bokelmann, 1995). *PP* and its precursors (yellow) sample the highest regions of the mantle, and the steeply incident PKP_{df} and PKP_{cd} are imaged in red. Additionally, the nearly vertical arrival seen near -50 sec at 115° is likely the precritical inner-core reflection *PKiKP*. The polarization of P_{diff} (orange) is well imaged out to 120°. The amplitude stack images P_{diff} to greater ranges because changes in amplitude on a single component are less affected by noise than is waveform coherence across components. The polarization of P_{diff} coda remains similar to the main arrival until it encounters the contaminating effects of *PP* precursors or the inner-core phases.

Modeling

Previous attempts to model P_{diff} coda (Bataille and Lund, 1996; Tono and Yomogida, 1996) have involved multiple scattering near the CMB. Here we consider an alternative explanation: single scattering from heterogeneities distributed throughout the mantle such as was proposed by Hedlin *et al.* (1997) to explain PKP_{df} precursor observations. Some of the scattered arrivals that could contribute to P_{diff} coda are shown in Figure 1b. The following paths are used in our calculations: direct *P* scattered either above or below its turning point (e.g., *p.p*, *p.P* and *P.P* in our notation) and P_{diff} scattered at or above above the CMB into *P* or P_{diff}.

We assume evenly distributed random heterogeneities in the mantle and apply Chernov's acoustic theory (Chernov, 1960; Wu and Aki, 1985) to model scattering. This is a single-scattering theory that assumes that the heterogeneity is sufficiently weak so that the Born approximation is valid. Chernov theory is most readily implemented using geometrical ray theory to describe the energy both incident to and scattered from the heterogeneities. Our situation is complicated by the fact that P_{diff} cannot be modeled with simple

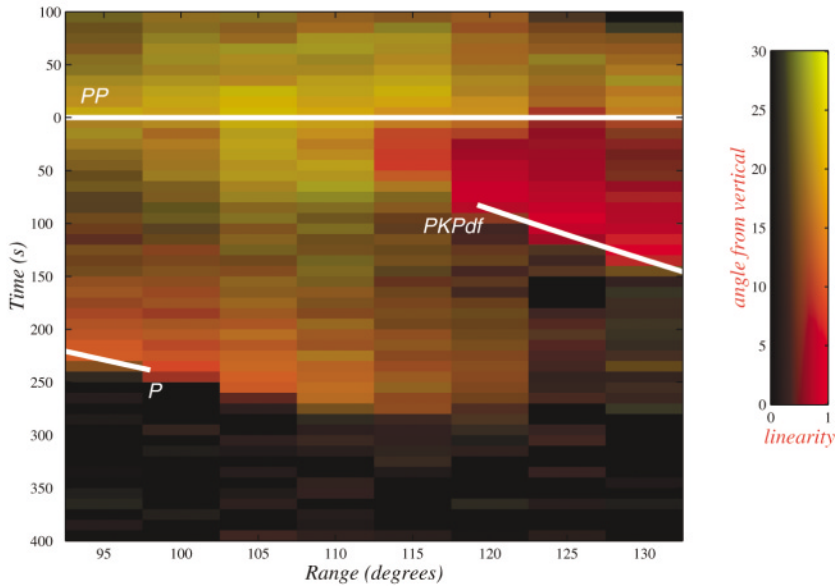

Figure 3. High-frequency (0.5 to 2.5 Hz) P_{diff} polarization and linearity in the radial vertical plane. The stack was generated using a bin size of 5° × 10 sec, and the data are plotted with respect to the theoretical *PP* arrival time. The color indicates the polarization angle, and the brightness is a function of the linearity. Only polarization angles between 0° and 30° are assigned colors; angles outside this range are black. The solid white lines show the theoretical arrival times of PKP_{df}, *PP*, and *P*.

ray theory. To obtain proper P_{diff} amplitudes in our calculations we implement a hybrid scheme that uses both reflectivity and three-dimensional ray theory. We use reflectivity-derived amplitudes for all rays that turn below 2300-km depth (including both deep-turning *P* and P_{diff}). We use the ray theoretical *PP* amplitude as a reference phase and calibrate our results to match the observed *PP* to *P* amplitude ratio at 80°.

The PREM velocity model (Dziewonski and Anderson, 1981) is used as a reference 1D velocity model. We do not explicitly account for attenuation; however, because attenuation for short-period *P* waves is dominated by the upper mantle (e.g., Warren and Shearer, 2000) and all of our arrivals have similar paths through the upper mantle, the effects of attenuation are largely accounted for by our *P*/*PP* amplitude calibration at 80°.

We divide the earth into 2° × 2° × 80-km voxels and parameterize the mantle velocity and density heterogeneity using an exponential autocovariance function. This leaves two free variables to model: the heterogeneity scale length and its rms amplitude. These variables control the amplitude and angular dependence of the scattered energy.

Synthetic envelopes are generated for a range of source-receiver distances by summing the energy contributions from all scattering paths that arrive in a given time–distance bin. Numerous voxels contribute energy to each bin. The resulting envelopes are the impulse responses of a PREM earth with only mantle heterogeneity.

Several additional effects have to be considered before these impulse–response functions can be compared to the data including the effects of near-surface scattering, source duration, and pulse broadening arising from factors discussed in the amplitude-stacking section. All these effects can be considered as an effective source term and accounted for by convolving the impulse response with an empirical source time function before comparing them to the data. Since we are modeling stacked traces the shape of this source time function should change little with increasing distance. Thus, we use a smooth version of the first 180 sec of the *P* wave and its coda observed at 80° as our source time function.

One possible problem with using this empirical source time function is that it not only contains the effects mentioned previously, but it also contains possible contributions from mantle scattering. However, the additional contribution from the mantle can be neglected because our modeling shows that at 80° the calculated amplitude of the mantle-scattered waves is less than 1% of observed coda amplitude and thus has little effect on the shape of the stacked envelope at 80°. At greater distances the theoretical contribution from the mantle scatterers increases.

Figure 4 demonstrates that the observations of P_{diff} coda are consistent with the hypothesis of evenly distributed mantle scatterers. The synthetics were generated using a scale length of 2 km with 1% rms velocity and density variations. These best-fitting values were obtained by trial and error.

Since the theory also provides the ray parameter of the energy arriving from all paths, we calculate the average slowness and compare it to the slownesses determined from the observed polarization angle. The polarization angle (θ) is converted to ray parameter (p) from the relation $p = \sin \theta/V$, where V is the average crustal velocity (6.0 km/sec).

Figure 5 shows the results. The particle-motion linearity (also plotted) indicates where the polarization angle measurements are robust. Overall, the model provides a reasonable fit to the data in regions with high linearity and no contaminating phases (see Fig. 3 for crossing arrivals).

Both the data and our calculations show P_{diff} coda arriving with a slowness similar to the main phase. The near constant slowness predicted by the whole-mantle scattering

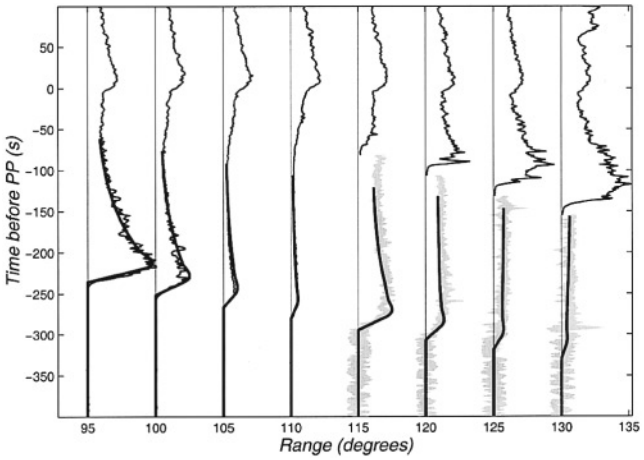

Figure 4. Amplitude stack with best-fitting calculated envelopes (smooth solid lines). The data stack is identical to that shown in Figure 2 except the width of magnified traces is equal to the two sigma error estimated using bootstrap resampling (Efron and Tibshirani, 1991).

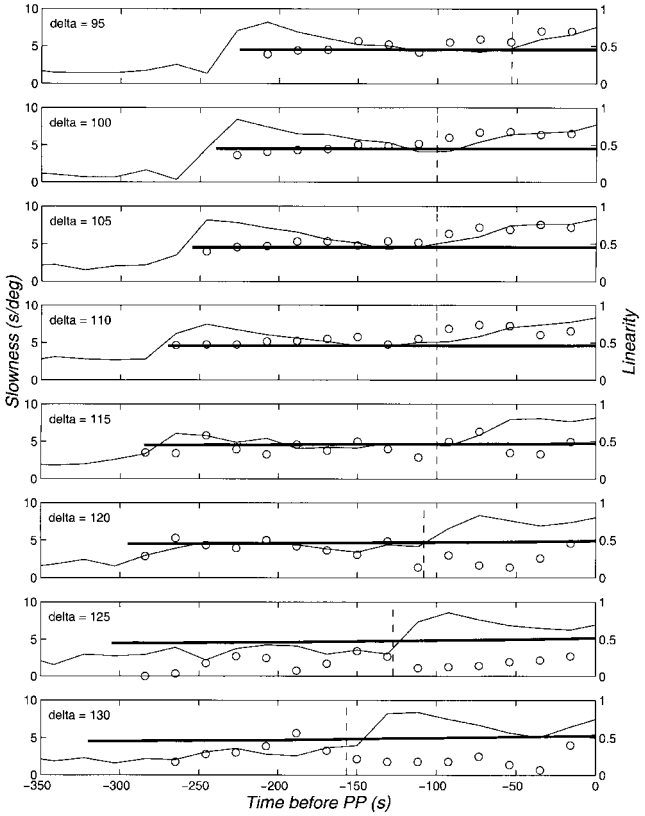

Figure 5. Observed and predicted slownesses of P_{diff} coda. The slowness calculated from the whole-mantle scattering model (thick solid lines) agrees reasonably well with the values obtained from the observed polarization angle (open circles) for times preceding the contaminating effects of *PP* precursors or *PKP* (dashed vertical lines) when the linearity (thin solid line) is high. The contamination onset times were estimated by picking the time on the amplitude stack (Fig. 2) when the energy starts to increase.

model arises mainly from two factors. First, scattered energy is focused in the forward direction for the parameters used in our model. Thus, energy scattered to paths and slownesses similar to the main phase will contribute the most energy to the coda. Second, the long duration of the source time function resulting from near surface scattering prolongs a uniform slowness.

As previously mentioned, our modeling assumes the heterogeneity is small enough that the effects of multiple scattering can be neglected; in addition the Born approximation assumes there is no reduction in the amplitude of the primary phase after scattering. It is possible given the great distances P_{diff} travels that these effects cannot be neglected.

Therefore, our heterogeneity magnitude estimate of 1% probably represents an upper bound because loss of P_{diff} energy due to scattering would increase the observed coda to a P_{diff} amplitude ratio. Similarly, our 2-km scale length would be a lower bound because multiple scattering would contribute more energy later in the P_{diff} coda, and the calculated envelopes for scale lengths greater than 2 km show less coda energy.

Discussion

To place our results in context of the ongoing debate over the depth distribution of fine-scale mantle structure, we briefly summarize previous results and discuss areas of consensus and contention. For a more complete treatment see Shearer *et al.* (1998) and Bataille *et al.* (1990) and the references therein.

The majority of research into the depth distribution of fine-scale mantle structure has focused on *PKP* precursors. These precursors originate from PKP_{df} scattering in the mantle before entering or after exiting the outer core. The onset times of these precursors require fine-scale structure at or immediately above the CMB. However, disagreement continues over how far the scatterers extend into the mantle. To determine this, one must model the entire waveform of the precursor. The greatest sensitivity to scattering higher in the mantle occurs at ranges close to the *PKP* "b" caustic and at times later in the precursory wave train.

The debate over the location of the fine-scale structure that generates PKP_{df} precursors began shortly after Haddon (1972) introduced the scattering origin for the precursors. For example, Doornbos and Vlaar (1973) inferred scatterers distributed up to 900 km above the CMB, and Haddon and Cleary (1974) countered that the scattering may actually be confined to a layer less than 200 km thick on top of the CMB. Doornbos (1978) and Bataille and Flatte (1988) presented an alternative origin for the PKP_{df} precursors. They showed scattering from topography on the CMB of a few hundred meters can produce energy levels consistent with the PKP_{df} precursor observations.

In a more recent study, Hedlin *et al.* (1997) compared a stack of 1600 seismograms that imaged the time–distance behavior of PKP_{df} precursors to the theoretical predictions from three models. The first model consisted of only CMB topography, the second contained a 200-km-thick layer of scatterers above the CMB, and the third contained scatterers distributed throughout the mantle. The best fit was found for the model containing scatterers distributed throughout the mantle. Cormier (1999) modeled the Hedlin *et al.* (1997) observations with a more complete single-scattering theory and found that about 1% velocity variations must extend at least 1000 km above the CMB to explain the time dependence in the precursor amplitudes.

The advantage of PKP_{df} precursor studies is that the precursors are uniquely sensitive to deep mantle scattering because shallow scattering contributes only to the PKP_{df} coda. However, their sensitivity to scattering in the middle and upper mantle is limited by the onset of the main *PKP* phase, making it difficult to determine precisely how far above the CMB the scattering extends. It is also not clear whether multiple scattering limited to near the CMB might also be able to explain the observations. The majority of the previously mentioned studies assumed single scattering, and even though this approximation has been shown valid for scatterers distributed throughout D″ (Cormier, 1995), its validity for the whole mantle remains untested. More general methods of calculating theoretical PKP_{df} precursors that incorporate multiple scattering are being refined and implemented (e.g., Cormier, 1995; Margerin *et al.*, 2000; Thomas *et al.*, 2000).

In addition to refining the modeling of PKP_{df} precursors, the debate over the depth extent of fine-scale heterogeneity can be advanced by the study of other high-frequency scattered arrivals. Scattered arrivals from a number of phases have been identified, including *PKKP*, *PP*, *PKPPKP*, and the target of the current study, P_{diff}.

Scattered *PKKP* waves have been used to place upper bounds of a few hundred meters on rms CMB topography (Doornbos, 1980; Earle and Shearer, 1997) but its use to constrain the possible depth extent of mantle scatterers remains untapped. King *et al.* (1975) showed the onset times, duration, slowness, azimuth, and amplitude variations of *PP* precursors can be explained by a 100-km scattering layer in the uppermost mantle and crust. The significant increase in global waveform data since 1975 warrants a reinvestigation of *PP* precursors to see if scattering contributions from deeper in the mantle can now be detected. Similar to *PP* precursors, *PKPPKP* precursors with lead times less than about 90 sec also primarily originate from uppermantle scattering (Haddon *et al.*, 1977).

In this work we show P_{diff} coda observations can be explained by a simple model with heterogeneity distributed throughout the mantle. This provides an alternative model to the results of Bataille and Lund (1996) and Tono and Yomogida (1996), who showed that multiple scattering near the CMB also generates a protracted P_{diff} coda. We conclude that observations of P_{diff} coda do not provide unique constraints on the depth distribution of scatterers in the mantle. However, they still may provide useful constraints if used in combination with observations of other scattered waves.

Conclusion

Our modeling shows that a mantle containing evenly distributed fine-scale heterogeneity can explain the average amplitude and polarization of P_{diff} coda. Multiple-scattering models with heterogeneity restricted to lowermost mantle (Bataille and Lund, 1996; Tono and Yomogida, 1996) could likely also satisfy our observations. However, the good fits shown in Figures 4 and 5 underscore the importance of considering structure higher in the mantle when studying high-frequency scattered arrivals (e.g., Hedlin *et al.*, 1997).

Future progress to determine the depth distribution of fine-scale mantle heterogeneity should include simultaneous modeling of different scattered phases, possibly including *PP* precursors, PKP_{df} precursors, and P_{diff} coda using a more complete scattering theory (e.g., Cormier, 1995; Margerin *et al.*, 2000; Thomas *et al.*, 2000). In addition, tighter observational constraints may arise from array analysis of the scattered phases.

Acknowledgments

We are grateful for suggestions and reviews from John Castle, George Choy, Jim Dewey, and Ed Garnero that improved the manuscript, and we thank the GSN and IRIS for collecting and distributing the data.

References

Bataille, K., and S. M. Flatte (1988). Inhomogeneities near the core-mantle boundary inferred from short-period scattered PKP waves recorded at the global digital seismograph network, *Geophys. Res. Lett.* **93,** 15,057–15,064.

Bataille, K., and F. Lund (1996). Strong scattering of short-period seismic waves by the core-mantle boundary and the P-diffracted wave, *Geophys. Res. Lett.* **23,** 2413–16.

Bataille, K., R. S. Wu, and S. M. Flatte (1990). Inhomogeneities near the core-mantle boundary evidenced from scattered waves: a review, *Pure. Appl. Geophys.* **132,** 151–173.

Bokelmann, G. H. R. (1995). *P*-wave array polarization analysis and effective anisotropy of the brittle crust, *Geophys. J. Int.* **120,** 145–162.

Chernov, L. A. (1960). *Wave Propagation in a Random Medium*, McGraw-Hill, New York.

Cormier, V. F. (1995). Time-domain modelling of PKIKP precursors for constraints on the heterogeneity in the lowermost mantle, *Geophy. J. Inter.* **121,** 725–736.

Cormier, V. F. (1999). Anisotropy of heterogeneity scale lengths in the lower mantle from PKIKP precursors., *Geophys. J. Int.* **136,** 373–384.

Dainty, A. M. (1990). Studies of coda using array and three-component processing, *Pageoph* **132,** 221–244.

Doornbos, D. J. (1978). On seismic-wave scattering by a rough core-mantle boundary, *Geophys. J. R. Astr. Soc.* **53,** 643–662.

Doornbos, D. J. (1980). The effect of a rough core–mantle boundary on PKKP, *Phys. Earth Planet. Interiors* **21,** 351–358.

Doornbos, D. J., and N. J. Vlaar (1973). Regions of seismic wave scattering in the Earth's mantle and precursors to PKP, *Nature* **243,** 58–61.

Dziewonski, A. M., and D. L. Anderson (1981). Preliminary reference Earth model., *Phys. Earth Planet. Interiors* **25,** 297–356.

Earle, P. S. (1999). Polarization of the Earth's teleseismic wavefield, *Geophys. J. Int.* **139,** 1–8.

Earle, P. S., and P. M. Shearer (1994). Characterization of global seismograms using an automatic-picking algorithm, *Bull. Seism. Soc. Am.* **84,** 366–376.

Earle, P. S., and P. M. Shearer (1997). Observations of *PKKP* precursors used to estimate small-scale topography on the core-mantle boundary, *Science* **277,** 667–670.

Efron, B., and R. Tibshirani (1991). Statistical data analysis in the computer age, *Science* **253,** 390–395.

Garnero, E. J. (2000). Heterogeneity of the lowermost mantle, *Annu. Rev. Earth Planet. Sci.* **28,** 509–537.

Haddon, R. A. W. (1972). Corrugations on the CMB or transition layers between inner and outer cores? *EOS* 600.

Haddon, R. A. W., and J. R. Cleary (1974). Evidence for scattering of seismic PKP waves near the mantle-core boundary, *Phys. Earth Planet. Interiors* **8,** 211–234.

Haddon, R. A. W., E. S. Husebye, and D. W. King (1977). Origins of precursors to $P'P'$, *Phys. Earth Planet. Interiors* **14,** 41–70.

Hedlin, M. A. H., and P. M. Shearer (2000). An analysis of large-scale variations in small-scale mantle heterogeneity using global seismographic network recordings of precursors to PKP, *J. Geophys. Res.* **105,** 13,655–13,673.

Hedlin, M. A. H., P. M. Shearer, and P. S. Earle (1997). Seismic evidence for small-scale heterogeneity throughout the earth's mantle, *Nature* **387,** 145–150.

Jurkevics, A. (1988). Polarization analysis of three-component array data, *Bull. Seism. Soc. Am.* **78,** 1725–1743.

Kanasewich, E. R. (1981). *Time Sequence Analysis in Geophysics*, The University of Alberta Press, Edmonton, Alberta, Canada.

Kennett, B. L. N., and E. R. Engdahl (1991). Traveltimes for global earthquake location and phase identification, *Geophys. J. Int.* **105,** 429–465.

King, D. W., R. A. W. Haddon, and E. S. Husebye (1975). Precursors to *PP, Phys. Earth Planet. Interiors* **10,** 103–127.

Margerin, L., G. Nolet, and F. A. Dahlen (2000). Multiple scattering analysis of PKP precursors, *EOS* **81.**

Shearer, P. M. (1991). Constraints on upper mantle discontinuities from observations of long-period reflected and converted phases, *J. Geophys. Res.* **96,** 18,147–18,181.

Shearer, P. M., M. A. H. Hedlin, and P. S. Earle (1998). PKP and PKKP precursor observations; implications for the small-scale structure of the deep mantle and core, in *The Core-Mantle Boundary Region*, M. Gurnis, M. Wysession, E. Knittle, and B. Buffet (Editors), Am. Geophys. Union Monograph **28,** 37–55.

Thomas, C., H. Igel, M. Weber, and F. Scherbaum (2000). Acoustics simulation of P-wave propagation in a heterogeneous spherical earth; numerical method and application to precursor wave to PKPdf, *Geophys. J. Int.* **141,** 307–320.

Tono, Y., and K. Yomogida (1996). Complex scattering at the core-mantle boundary observed in short-period diffracted P-waves, *J. Phys. Earth* **44,** 729–744.

Vidale, J. E., and A. H. Hedlin (2000). Evidence for partial melt at the core-mantle boundary north of Tonga from the strong scattering of seismic waves, *Nature* **391,** 682–685.

Warren, L. M., and P. M. Shearer (2000). Investigating the frequency dependence of mantle Q by stacking P and PP spectra, *J. Geophys. Res.* **105,** 25,391–25,402.

Wen, L., and D. Helmberger (1998). Ultra-low velocity zones near the core-mantle boundary from broadband PKP precursors, *Science* **279,** 1701–1703.

Wu, R., and K. Aki (1985). Elastic wave scattering by a random medium and the small-scale inhomogeneities in the lithosphere, *J. Geophys. Res.* **90,** 10,261–10,273.

U.S. Geological Survey
MS 966 Box 25046 DFC
Denver, Colorado 80225
(P.S.E.)

Scripps Institution of Oceanography, SIO-0225
La Jolla, California 92093-0225
(P.M.S.)

Manuscript received 5 December 2000.